Synthesis and Characterization of Allosteric Probes of Substrate Channeling in the Tryptophan Synthase Bienzyme Complex[†,‡]

Huu Ngo,[§] Rodney Harris,[§] Novelle Kimmich,[§] Patricia Casino,[§] Dimitri Niks,[§] Lars Blumenstein,[∥] Thomas Reinier Barends,[∥] Victor Kulik,[∥] Michael Weyand,[⊥] Ilme Schlichting,[∥] and Michael F. Dunn*[,§]

Department of Biochemistry, University of California, Riverside, California 92521, Department of Biomolecular Mechanisms, Max Planck Institute for Medical Research, Heidelberg, Germany, and Department of Biophysical Chemistry, Max Planck Institute of Molecular Physiology, Dortmund, Germany

Received February 25, 2007; Revised Manuscript Received April 17, 2007

ABSTRACT: Allosteric interactions regulate substrate channeling in *Salmonella typhimurium* tryptophan synthase. The channeling of indole between the α- and *β*-sites via the interconnecting 25 Å tunnel is regulated by allosteric signaling arising from binding of ligand to the α-site, and covalent reaction of L-Ser at the *β*-site. This signaling switches the α- and *β*-subunits between open conformations of low activity and closed conformations of high activity. Our objective is to synthesize and characterize new classes of α-site ligands (ASLs) that mimic the binding of substrates, 3-indole-D-glycerol 3′-phosphate (IGP) or D-glyceraldehyde 3-phosphate (G3P), for use in the investigation of α-site−*β*-site interactions. The new synthesized IGP analogues contain an aryl group linked to an *O*-phosphoethanolamine moiety through amide, sulfonamide, or thiourea groups. The G3P analogue, thiophosphoglycolohydroxamate, contains a hydroxamic acid group linked to a thiophosphate moiety. Crystal structures of the internal aldimine complexed with G3P and with three of the new ASLs are presented. These structural and solution studies of the ASL complexes with the internal aldimine form of the enzyme establish the following. (1) ASL binding occurs with high specificity and relatively high affinities at the α-site. (2) Binding of the new ASLs slows the entry of indole analogues into the *β*-site by blocking the tunnel opening at the α-site. (3) ASL binding stabilizes the closed conformations of the *β*-subunit for the α-aminoacrylate and quinonoid forms of the enzyme. (4) The new ASLs exhibit allosteric properties that parallel the behaviors of IGP and G3P.

Tryptophan synthase from *Salmonella typhimurium* consists of an $\alpha_2\beta_2$ bienzyme complex with α*β* dimeric units assembled as the tetrameric species via the *β*−*β* subunit interface (*1*−*6*). Each α-subunit catalyzes the cleavage of 3-indole-D-glycerol 3′-phosphate (IGP)[1] to indole and D-glyceraldehyde 3-phosphate (G3P) (Scheme 1A). The indole produced at the α-site within an α*β* dimeric unit is transferred to the *β*-subunit via a 25 Å long interconnecting tunnel (*7*). The pyridoxal phosphate requiring *β*-subunit then catalyzes a *β*-replacement reaction in which indole replaces the hydroxyl of L-Ser, giving L-Trp (Scheme 1B).

Substrate channeling in the tryptophan synthase bienzyme complex is regulated by allosteric interactions that ensure the efficient utilization of IGP for the conversion of L-Ser to L-Trp. While the broad outlines of this allosteric regulation have been established (*5*, *6*, *8*−*20*), the detailed allosteric mechanism has not been determined.

[†] Supported by NIH Grant GM5574 (M.F.D.) and Deutsche Forschungsgemeinschaft (I.S.).

[‡] Structure factors and coordinates have been submitted to the Protein Data Bank as entries 2CLK, 2CLE, 2CLF, 2CLI, and 2CLH.

* To whom correspondence should be addressed: Department of Biochemistry, University of California, Riverside, CA 92521. Phone: (951) 827-4235. Fax: (951) 827-4434. E-mail: michael.dunn@ucr.edu.

[§] University of California.

[∥] Max Planck Institute for Medical Research.

[⊥] Max Planck Institute of Molecular Physiology.

Conformational Triggers

The binding of substrate, IGP, product, G3P, or analogues of these ligands to the α-site switches the α-subunit to a closed conformation (*6*−*13*, *17*−*19*, *21*−*24*). The IGP-mediated switch to the closed conformation of the α-site triggers an allosteric transition within the *β*-subunit that alters the distribution of intermediates at the *β*-site and changes activation energies for the interconversion of intermediates in stages I and II of the *β*-reaction (*16*). This IGP-mediated

[1] Abbreviations: $\alpha_2\beta_2$, native form of tryptophan synthase from *S. typhimurium*; α, α-subunit; *β*, *β*-subunit; E(Ain), internal aldimine (Schiff base) intermediate; E(Aex_1), external aldimine intermediate formed between the PLP cofactor and L-Ser; E(GD), gem diamine species; E(A−A), α-aminoacrylate Schiff base; E(Q_1), L-Ser quinonoid intermediate; E(Q_3), quinonoid intermediate that accumulates in the reaction between E(A−A) and indole; E(Aex_2), L-Trp external aldimine intermediate; PLP, pyridoxal phosphate; IGP, 3-indole-D-glycerol 3′-phosphate; GP, α-D,L-glycerol phosphate; G3P, D-glyceraldehyde 3-phosphate; ASL, α-site ligand; F6, *N*-(4′-trifluoromethoxybenzoyl)-2-aminoethyl phosphate; F9, *N*-(4′-trifluoromethoxybenzenesulfonyl)-2-aminoethyl phosphate; F12, *N*-(4′-trifluoromethylphenyl)-*N*′-(2-phosphoryloxyethyl)thiourea; F19, *N*-(naphthalene-2′-sulfonyl)-2-aminoethyl phosphate; F21, *N*-(4′-fluorobenzenesulfonyl)-2-aminoethyl phosphate; TPGH, thiophosphoglycolohydroxamate; ANS, 8-anilino-1-naphthalene sulfonate; TEA, triethanolamine; MVC, monovalent cation; K_{Dapp}, apparent dissociation constant. Structural elements of tryptophan synthase are designated as follows: loop αL2, α53−60; loop αL6, α179−193; helix αH8, α249−265; COMM domain, *β*102−189; helix *β*H5, *β*145−150; helix *β*H6, *β*165−181.

10.1021/bi700385f CCC: $37.00
Published on Web 06/09/2007

Scheme 1[a]

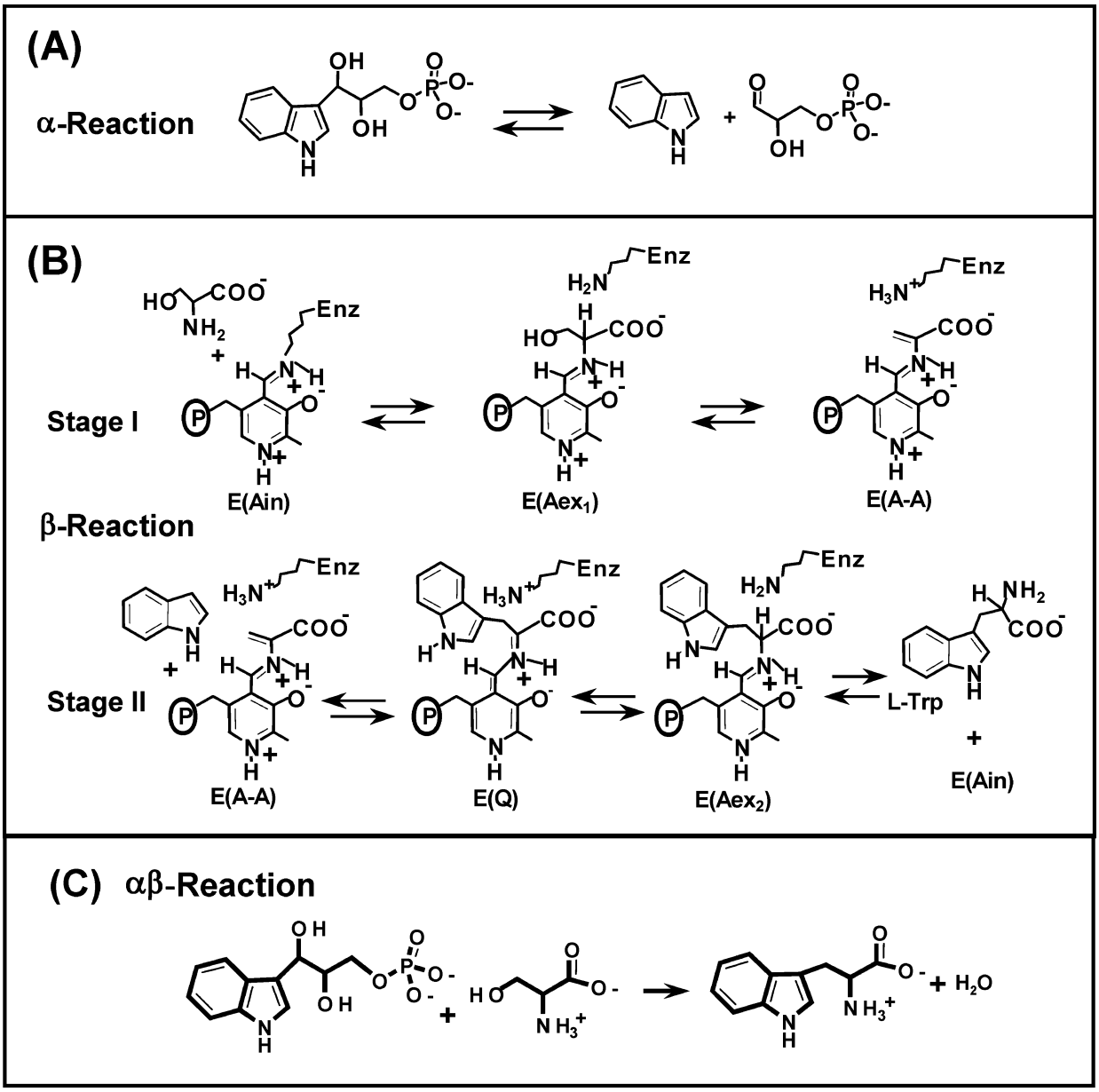

[a] (A) In the α-reaction, IGP is cleaved to give indole and G3P. (B) In the *β*-reaction, L-Ser reacts with enzyme-bound PLP to make E(A−A) in stage I, and then indole from the α-site reacts with E(A−A) to yield L-Trp in stage II. (C) α*β*-Reaction.

allosteric transition also favors the switching of the *β*-site to the closed conformation. When the L-Ser external aldimine intermediate, $E(Aex_1)$, is converted to the α-aminoacrylate intermediate, E(A−A), the *β*-subunit is switched to the closed conformation, and the α-site is activated for the cleavage of IGP (*9*). Conversion of the L-Trp quinonoid intermediate, E(Q), to the L-Trp external aldimine intermediate, $E(Aex_2)$ (Scheme 1B), switches off the activity of the α-site (*12*). This switching between low- and high-activity states and between open and closed conformations is critically important for the synchronization of catalysis at the α- and *β*-sites during the α*β* reaction (*6*, *8*, *9*, *12*−*14*, *17*). Despite the large amount of data that is available, the chemical and structural details of the ligand-mediated mechanism for switching between the open and closed conformations of the α- and *β*-subunits are not well-understood.

To further investigate the details of the allosteric mechanism that regulates substrate channeling, we introduce in this study five new IGP analogues (representing three new analogue classes) and one new G3P analogue [designated F6, F9, F12, F19, F21, and TPGH, respectively (Figure 1)]. Previous workers have introduced analogues of IGP and/or G3P for use in the study of tryptophan synthase (*24*−*27*). Four of the new ASL examples presented in this work (F6, F9, F12, and F21) incorporate ^{19}F spectroscopic probes intended ultimately for use in ^{19}F NMR spectroscopy. These four ligands have structures that link aromatic groups containing the spectroscopic probe to the amino group of *O*-phosphoethanolamine. The fifth ligand, a G3P analogue, TPGH, consists of a sodium thiophosphate moiety attached to *N*-acetylhydroxamic acid. Similar analogues have proven to be effective ligands for triosephosphate isomerase (*28*, *29*). Herein, we characterize the binding and allosteric effects of these ASLs on the *β*-site of tryptophan synthase by examining reactions involving L-Ser, indoline, and analogues of these substrates. We also determined crystal structures of

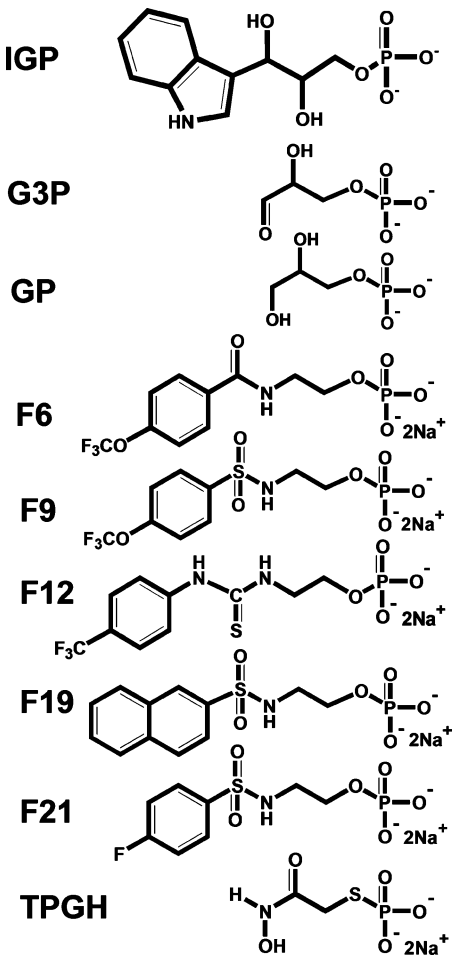

FIGURE 1: Chemical structures of the substrate, IGP, the product, G3P, and their analogues (GP, F6, F9, F12, F19, F21, and TPGH).

three of the new ASLs complexed with the internal aldimine form of the enzyme and compared these structures with the structure of the G3P complex and with the structures of previously determined ASL complexes. It will be shown that these new analogues exhibit structures, affinities, and allosteric properties that modulate substrate channeling in the tryptophan synthase system, rendering them interesting probes for investigation of the allosteric site−site interactions. This work is the first paper in a series (*30*, *31*) where these analogues are used in combination with optical spectroscopy, rapid kinetics, X-ray crystallography, and ^{19}F or ^{13}C NMR to develop a detailed mechanistic description of the allosteric regulation of tryptophan synthase.

MATERIALS AND METHODS

Materials

L-Serine, benzimidazole, 8-anilino-1-naphthalenesulfonate (ANS), α-glycerol phosphate (GP), *O*-phosphorylethanolamine (PEA), and the diethyl acetal of D-glyceraldehyde 3-phosphate were purchased from Sigma. Aliquots of G3P were prepared from the diethyl acetal according to the manufacturer's instructions, stored frozen at −78 °C, and thawed just prior to use. Indoline, 4-(trifluoromethoxy) benzoyl chloride, 4-(trifluoromethoxy)benzenesulfonyl chloride, 4-(trifluoromethyl) phenyl isothiocyanate, naphthalene-2-sulfonyl chloride, 4-fluorobenzenesulfonyl chloride, ethyl chloroacetate, hydroxylamine as a 50% by weight aqueous solution, sodium thiolphosphate dodecahydrate, and trimethanolamine (TEA) were purchased from Aldrich. Indoline was further purified as previously described (*17*). For studies in solution, purification of wild-type *S. typhimurium* $\alpha_2\beta_2$ tryptophan synthase and determination of protein concentration were accomplished as previously described (*16*, *32*−*36*). For the crystal structure determinations, tryptophan synthase was purified and crystallized as described in ref *26*.

Methods

UV−*Vis Absorbance Spectral Measurements.* Static UV−vis absorbance spectra and activity measurements were performed on a Hewlett-Packard 8452A diode array spectrophotometer at 25 ± 2 °C. All these experiments were carried out in 50 mM TEA buffer containing 100 mM NaCl (*14*) at pH 7.8. The binding of ligands to the α-site was followed by the changes in absorbance of intermediates bound to the β-site at the following wavelengths: 350 nm for E(A−A), 422 nm for E(Aex_1), and 466 nm for $E(Q)_{indoline}$.

UV−*Vis L-Ser Titration Studies*. Titrations of the enzyme with L-Ser were performed to determine the influence of the new ASLs on the apparent dissociation constants, K_{Dapp}, for the L-Ser reaction at 25 ± 2 °C in 50 mM TEA buffer containing 100 mM NaCl at pH 7.8. Measurements were carried out both in the absence and in the presence of different ASLs. The disappearance of E(Ain) species, with a λ_{max} of 412 nm, occurs when L-Ser is titrated into the solution. Titration plots of the absorbance at 412 nm versus the L-Ser concentration were fitted to a hyperbolic equation (eq 1):

$$\Delta A = (A_\infty - A_0)[\text{L-Ser}]/(K_{Dapp} + [\text{L-Ser}]) \qquad (1)$$

where ΔA is the observed absorbance change and A_0 and A_∞ are the absorbance values at [L-Ser] = 0 and [L-Ser] extrapolated to ∞, respectively.

Static Fluorescence Spectroscopy. Static fluorescence measurements were taken using a J-Y Spex Fluorolog II spectrofluorometer equipped with a 150 W Xe source. Titrations to determine the dissociation constants for binding of ligand to the E(Ain) and E(A−A) complexes were performed using the fluorescence probe, ANS (*21*). The excitation wavelength was set at 380 nm, and the emission spectra were collected over the wavelength range of 400−600 nm. The accompanying change in ANS fluorescence provides a sensitive signal that can be used to monitor the binding of ligands to the α-site. In this paper, the interactions of the ligands GP, G3P, F6, F9, F12, F19, F21, and TPGH with the α-site were investigated using ANS as the fluorescent probe. To ensure the total concentrations of enzyme and ANS remained invariant throughout the titrations, measurements were carried out at 25 ± 2 °C in 50 mM TEA buffer at pH 7.8 containing either 100 mM NaCl or 100 mM NaCl and 40 mM L-Ser, by the following methods. (a) Small aliquots of a solution containing 100 mM NaCl, 10 μM $\alpha_2\beta_2$ tryptophan synthase, 20 μM ANS, and concentrated ligand were added to a fluorescence cuvette equipped with a micro stir bar containing 100 mM NaCl, 10 μM $\alpha_2\beta_2$ tryptophan synthase, and 20 μM ANS, or (b) small aliquots of a solution containing 100 mM NaCl, 10 μM $\alpha_2\beta_2$ tryptophan synthase, 20 μM ANS, 40 mM L-Ser, and concentrated ligand were

added to a fluorescence cuvette equipped with a micro stir bar containing 100 mM NaCl, 10 μM $\alpha_2\beta_2$ tryptophan synthase, 20 μM ANS, and 40 mM L-Ser. Fluorescence amplitude measurements were analyzed by fitting the data to the equation for a rectangular hyperbola (eq 2)

$$\Delta F = (F_i - F_n)[\text{ligand}]/(K_{Dapp} + [\text{ligand}]) \qquad (2)$$

where ΔF is the observed change in fluorescence, F_n is the fluorescence extrapolated to ligand saturation, and F_i is the initial fluorescence value. When fitted to eq 2, plots of emission intensity at 500 nm versus the analogue concentration gave values for the apparent dissociation constant, K_{Dapp}.

Single-Wavelength Stopped-Flow (SWSF) Kinetic Studies. SWSF measurements at 25 ± 2 °C were taken as previously described (*14*). To quantify the effects of analogues on the indoline reaction rate, SWSF measurements were used to monitor the reaction at 466 nm. Analogues were preincubated in both syringes of the stopped-flow apparatus with the enzyme in one syringe and indoline in the other syringe. Typically, each syringe also contained 100 mM NaCl and 40 mM L-Ser. When the contents of the two syringes were mixed, the enzyme and the indoline concentrations were reduced by one-half in this mixing protocol.

^{1}H and ^{19}F NMR Spectroscopy. All ^{1}H and ^{19}F NMR spectra were recorded on a Varian 300 MHz spectrophotometer. All ligands were dissolved in D_2O, and experiments were carried out at 25 ± 2 °C. ^{1}H chemical shifts are reported relative to the HOD signal, and ^{19}F chemical shifts are reported relative to trifluoroacetate ion.

N-(4′-Trifluoromethoxybenzoyl)-2-aminoethyl Phosphate (F6). The synthesis of F6 was carried out by reaction of *O*-phosphorylethanolamine (PEA) with 4-(trifluoromethoxy) benzoyl chloride in aqueous solution under mildly basic conditions (pH ~8). In a typical preparation, 6 mmol of PEA and 18 mmol of NaOH were dissolved in 2 mL of water in an Erlenmeyer flask. To this stirred solution was added dropwise 6 mmol of 4-(trifluoromethoxy) benzoyl chloride. The mixture turned cloudy immediately upon addition of 4-(trifluoromethoxy) benzoyl chloride. The resulting mixture was stirred for 2 h at room temperature, then heated to 50 °C for 1 h, and finally cooled to room temperature and stirred overnight to ensure the completion of the reaction. To isolate the product, 6 mmol of $CaCl_2$ dissolved in 2 mL of water was added dropwise to the stirred mixture to precipitate the Ca^{2+} salt of the crude product, *N*-(4′-trifluoromethoxybenzoyl)-2-aminoethyl phosphate (F6). The precipitate was isolated by vacuum filtration and rinsed with water. Because of the considerably greater solubility of the Ca^{2+} salt of PEA, the Ca^{2+} salt of F6 was separated from excess PEA by washing the mixture of Ca^{2+} salts with four 20 mL aliquots of water to selectively dissolve the Ca^{2+} salt of PEA. The Ca^{2+} salt of F6 then was re-isolated by vacuum filtration and the process repeated. The purified Ca^{2+} salt of F6 was converted to the Na^+ salt by making a slurry of the Ca^{2+} salt with 10 g of the Na^+ form of chelating resin, Duolite 476, in 30 mL of water. The slurry was swirled on a shaker for 12 h or until the F6 precipitate completely dissolved as the exchange of Na^+ for Ca^{2+} occurred. Upon completion of the exchange, the highly soluble Na^+ salt of F6 was separated from the chelating resin by vacuum filtration. The filtrate was frozen in an acetone/dry ice bath and then lyophilized to yield the Na^+ salt of F6 as a white powder (yield, 65%). The organic content of this powder was shown to be more than 96% F6 by one-dimensional ^{1}H NMR. The observed amplitudes, chemical shifts, and *J* coupling [^{1}H NMR δ 3.6 (2H, triplet, J = 5.4 Hz), 3.8 (2H, quartet, J = 5.8 Hz), 7.4 (2H, doublet, J = 8.7 Hz), 7.8 (2H, doublet, J = 8.7 Hz), ^{19}F NMR δ 17.8 (singlet)] confirm the structural assignment.

N-(4′-Trifluoromethoxybenzenesulfonyl)-2-aminoethyl Phosphate (F9). The synthesis of F9 was accomplished using a synthetic protocol similar to that described above for F6. F9 was prepared by reaction of PEA with 4-(trifluoromethoxy)-benzenesulfonyl chloride. In a typical preparation, 3 mmol of PEA and 9 mmol of NaOH were dissolved in 1 mL of water in an Erlenmeyer flask. To this stirred solution was added dropwise 3 mmol of 4-(trifluoromethoxy)benzenesulfonyl chloride. The mixture was stirred overnight to ensure the completion of the reaction. After 14 h, 8 mL of water was added to dissolve the white precipitate, giving a homogeneous solution. Then 3 mmol of $CaCl_2$ dissolved in 1 mL of H_2O was added to the homogeneous solution of crude F9. The purification process was the same as that for F6. The yield of the purified Na^+ salt was >55%. One-dimensional ^{1}H NMR spectroscopy established that the purity of F9 was >98%; the amplitudes, chemical shifts, and *J* coupling [^{1}H NMR δ 3.12 (2H, triplet, J = 5.4 Hz), 3.8 (2H, quartet, J = 5.8 Hz), 7.6 (2H, doublet, J = 8.8 Hz), 8.0 (2H, doublet, J = 8.9 Hz), ^{19}F NMR δ 17.7 (singlet)] were found to be consistent with the assigned structure.

N-(4′-Trifluoromethylphenyl)-N′-(2-phosphoryloxyethyl)-thiourea (F12). The synthesis of F12 was accomplished using a synthetic protocol slightly different from the methodologies described above for F6 and F9. F12 was synthesized by dissolving 5 mmol of PEA and 10 mmol of NaOH in 2 mL of water in an Erlenmeyer flask. To this stirred solution was added dropwise 5 mmol of 4-(trifluoromethyl)phenyl isothiocyanate (dissolved in 600 μL of CH_3CN). The mixture was heated for 2 h at 50 °C, then cooled to room temperature, and stirred overnight to ensure the completion of the reaction. Finally, 5 mmol of $CaCl_2$ dissolved in 2 mL of water was added dropwise to the stirred mixture to precipitate the Ca^{2+} salt of the crude product (F12). The purification steps were the same as those used for F6. The purified Na^+ salt of the product was obtained in >47% yield. One-dimensional ^{1}H NMR spectroscopy confirmed that the purity of F12 was >90%; the amplitudes, chemical shifts, and *J* coupling [^{1}H NMR δ 3.15 (2H, triplet, J = 5.2 Hz), 3.9 (2H, quartet, J = 5.14 Hz), 7.55 (2H, doublet, J = 8.4 Hz), 7.77 (2H, doublet, J = 8.6 Hz), ^{19}F NMR δ 13.5 (singlet)] confirm the structural assignment.

N-(Naphthalene-2′-sulfonyl)-2-aminoethyl Phosphate (F19). The synthesis of F19 was accomplished using a synthetic protocol similar to the methodology described above for F12. F19 was synthesized by dissolving 3 mmol of PEA and 9 mmol of NaOH in 1 mL of water in an Erlenmeyer flask. To this stirred solution was added dropwise 3 mmol of naphthalene-2-sulfonyl chloride (dissolved in 3 mL of CH_3CN). A white precipitate slowly formed, and the mixture was allowed to react overnight to ensure the completion of the reaction. The purification steps were the same as those used for F6. The purified Na^+ salt of the product was obtained in >65% yield. One-dimensional ^{1}H NMR spec-

troscopy confirmed that the purity of F9 was >95%; the amplitudes, chemical shifts, and *J* coupling [^{1}H NMR δ 3.12 (2H, triplet, $J = 5.4$ Hz), 3.8 (2H, quartet, $J = 5.7$ Hz), 7.7 (2H, triplet, $J = 6.9$ Hz), 7.85 (1H, doublet, $J = 8.7$ Hz), 8.05 (3H, doublet, $J = 9.1$ Hz), 8.45 (1H, singlet)] were found to be consistent with the assigned structure.

N-(4′-Fluorobenzenesulfonyl)-2-aminoethyl Phosphate (F21). F21 was synthesized by reaction of 4-fluorobenzenesulfonyl chloride with PEA using the same protocol as described above for F9. One-dimensional ^{1}H NMR spectroscopy established that the purity of F21 was >98%. The amplitudes, chemical shifts, and *J* coupling for the aliphatic region are as follows: δ 3.12 (2H, triplet, $J = 5.4$ Hz), 3.79 (2H, quartet, $J = 5.8$ Hz). The aromatic region of the ^{1}H spectrum is consistent with an expected A_2B_2C spin system (where C = F) involving the two ortho and two meta protons and the para fluorine. The aromatic region of the ^{1}H spectrum shows a multiplet of at least three lines with chemical shifts of 7.393, 7.364, and 7.334 ppm and a multiplet of at least seven lines with chemical shifts of 7.974, 7.967, 7.957, 7.950, 7.944, 7.939, and 7.927 ppm. The ^{19}F spectrum exhibited a symmetric mutliplet consisting of seven lines with chemical shifts (relative to trifluoroacetate ion) of −30.415, −30.227, −30.239, −30.251, −30.263, −30.275, and −30.288 ppm.

Thiophosphoglycolohydroxamate (TPGH). TPGH was synthesized by a two-step reaction sequence based on the procedures of Jones and Werner (*37*) and Duncan and Drueckhammer (*38*) with minor modifications. The first step involved preparation of monochloroacethydroxamic acid by reaction of ethyl chloroacetate with hydroxylamine. Hydroxylamine (12 mmol), as a 50% by weight aqueous solution (Aldrich), was added slowly with stirring to 12 mmol of ethyl chloroacetate in a round-bottom flask. The mixture was stirred for 5 min at room temperature and then cooled in an ice bath for 15 min. Further stirring at room temperature for 3 h gave a product mixture containing a yellow precipitate. The resulting mixture was then filtered, giving a yellow solid, presumed to be crude monochloroacetohydroxamic acid. TPGH was then prepared by reacting this material with thiophosphate ion as follows. To a solution of 2.1 mmol of crude monochloroacetohydroxamic acid (dissolved in 1 mL of H_2O) was added dropwise 3.2 mmol of sodium thiophosphate dodecahydrate (dissolved in 8 mL of H_2O). The resulting mixture was stirred for 1 h, and then 2.1 mmol of $CaCl_2$ was added to precipitate TPGH as the insoluble Ca^{2+} salt. The Ca^{2+} salt of TPGH was purified and converted to the Na^+ salt using the same protocol employed above in the preparation of the Na^+ salt of F6. One-dimensional ^{1}H NMR spectroscopy established that the purity of TPGH was >95%. The amplitudes and chemical shifts [δ 3.21 (1H, singlet), 3.24 (1H, singlet)] verified the structural assignment.

Crystallization, Complex Formation, Diffraction Data Collection, and Refinement. Complex formation was achieved by soaking native crystals for 10 min in a solution containing 90 mM Bis-Tris-Propane (pH 7.8), 150 mM NaCl, 15% (w/v) PEG 8000, 20% glycerol, and 10 mM F9 or F19. The F6 complexes were made analogously using either 10 or 66 mM F6, yielding complexes designated as low-F6 or high-F6, respectively. The G3P complex was obtained by soaking crystals for 40 min in a solution containing 28 mM Na^+-Hepes (pH 7.0), 12% (w/v) PEG 8000, 30 mM Na-G3P, and 20% glycerol before the mixture was cryo-cooled in liquid nitrogen. Diffraction data were collected at the European Synchrotron Radiation Facility (ESRF, Grenoble, France) as listed in Table 1, with the crystal kept at 100 K. The data were processed with the XDS suite of programs (*39*). The starting model used for the refinement of the enzyme complexes was a coordinate set for the IPP complex with E(Ain) (PDB entry 1QOP) but with the coordinates of loops αL2 and αL6, IPP, PLP, the sodium ion, and all water molecules omitted. For each structure, the initial model was divided into three substructures [α-subunit, COMM domain (*26*), and the core of the β-subunit] and subjected to rigid body and simulated annealing refinement by CNS 1.0 or CNS 1.1 (*40*). Clear electron density was observed for G3P, F6, F9, F19, and the PLP molecule after the first cycle of simulated annealing refinement. Thus, these parts of the structure were included in the subsequent refinement steps. This was also true for loops αL2 and αL6 in the G3P, F9, and F19 complexes with E(Ain). In the F6 complexes, loop αL6 is rather disordered and, therefore, was not included in the refinement. Coordinates for water molecules were found mostly automatically using the CNS 1.1 module WATERPICK. The occupancy for all solvent atoms was kept at unity throughout the refinement. Structures were superimposed with O (*41*) and Xfit (*42*) using all common C_α atoms for each pair of structures except for the C_α atoms belonging to loop αL2, loop αL6, and the COMM domain. During the course of the refinement of the high-F6 complex, it became apparent that there is a second, partially occupied position for an F6 molecule. Its occupancy was set to 0.5.

RESULTS

Static Studies

Influence of ASL Binding on the Spectra of Intermediates Bound to the β-Site in the L-Ser Reaction. Figure 2A, spectrum a, shows the PLP cofactor region of the absorbance spectrum of $\alpha_2\beta_2$ alone in TEA. The band at 412 nm (shoulder at ∼330 nm) has been assigned to the internal aldimine, E(Ain) (*1*). This spectrum changes upon addition of L-Ser and the ASLs. Spectra b and c are the absorbance spectra of the PLP chromophore after the reaction of L-Ser with $\alpha_2\beta_2$ has reached equilibrium in the absence (b) and presence (c) of 50 mM GP. In the absence of GP (spectrum b), the spectrum shows that the equilibrium distribution of intermediates in stage I of the β-reaction is dominated by two species, E(Aex$_1$) ($\lambda_{max} = 422$ nm) and E(A−A) ($\lambda_{max} =$ 350 nm, shoulder extending to >500 nm) (*43*, *44*). The binding of GP (spectrum c) causes a redistribution in which there is a decrease in the amount of E(Aex$_1$) and a corresponding increase in the amount of E(A−A) (*8*, *44*). This behavior can be seen more clearly in the difference spectrum (spectrum e) generated by subtracting spectrum b from spectrum c. There is a large positive absorbance at 350 nm that corresponds to an increase in the level of E(A−A) and a large negative absorbance at 412 nm due to a decrease in the level of E(Aex$_1$).

The spectra in panels B and C of Figure 2 establish that the binding of G3P or F9 also causes changes in the spectrum of the PLP chromophore, and the changes are similar to the changes caused by GP. Figure 2D summarizes the changes in the redistribution of species caused by GP, G3P, TPGH,

Table 1: Crystal Parameters, Data Collection, and Refinement Statistics

	(G3P)E(Ain)	(F6)E(Ain) low	(F6)E(Ain) high	(F9)E(Ain)	(F19)E(Ain)
PDB entry	2CLK	2CLE	2CLF	2CLI	2CLH
Crystal Parameters					
space group	*C*2	*C*2	*C*2	*C*2	*C*2
unit cell dimensions					
a, *b*, *c* (Å)	182.0, 59.6, 67.4	182.4, 59.6, 67.2	182.0, 59.6, 67.4	182.8, 59.0, 67.4	181.6, 59.0, 67.0
β (deg)	94.56	94.74	94.56	94.78	94.63
Data Collection					
beamline	14-1	14-3	14-1	14-1	14-3
X-ray source	ESRF	ESRF	ESRF	ESRF	ESRF
wavelength (Å)	0.934	0.931	0.934	0.931	0.931
Data Statistics					
resolution (Å)	20−1.5	20−1.5	19.2−1.6	19.9−1.7	19.6−1.7
no. of observations	212704	349774	519911	340984	244889
no. of unique reflections	107933	1267111	90154	90393	76588
completeness (total/high) (%)[a]	93.7/83.1	89.5/95.7	95.4/73.3	95.7/83.5	98.1/95.4
$\langle I/\sigma(I)\rangle$ (total/high)[a]	8.3/1.9	11.4/2.3	11.9/3.2	10.3/2.2	10.5/2.3
R_{sym} (total/high)[a,b]	5.5/23.4	5.0/37.3	11/50	8.1/55.1	8.1/37.4
Refinement Statistics					
resolution range (Å)	10−1.5	10−1.5	19.15−1.7	10−1.7	18−1.7
refinement program	REFMAC	CNS 1.1	CNS1.1	CNS1.0	CNS1.1
included amino acids	A 1−267	A 1−178	A 1−178	A 1−184	A 1−184
	B 2−391	A 194−268	A 194−268	A 195−267	A 194−267
		B 2−395	B 2−395	B 2−395	B 2−395
no. of protein atoms	5510	4887	4864	4870	4933
no. of waters	530	600	625	601	552
no. of ligand atoms	25	36	58	36	36
no. of Na^+ ions	1	1	1	1	1
R_{work} (%)[c]	17.9	19.4	17.6	18.8	19.6
R_{free} (%)[d]	20.2	21.0	19.6	20.6	22.0
rms deviation for bonds (Å)	0.023	0.005	0.006	0.005	0.005
rms deviation for angles (deg)	2.10	1.36	1.39	1.20	1.30

[a] Completeness, R_{sym}, and $\langle I/\sigma(I)\rangle$ are given for all data and for the highest-resolution shell. Resolution shells are 1.5−1.6 Å for G3P, 1.5−1.6 Å for the low-F6 complex, 1.7−1.8 Å for the high-F6 complex, 1.7−1.8 Å for F9, 1.7−1.8 Å for F19. [b] $R_{sym} = \sum|I - \langle I\rangle|/\sum I$. [c] $R_{work} = \sum|F_{obs}| - k|F_{calc}|/\sum|F_{obs}|$. [d] Five percent of randomly chosen reflections were used for the calculation of R_{free}.

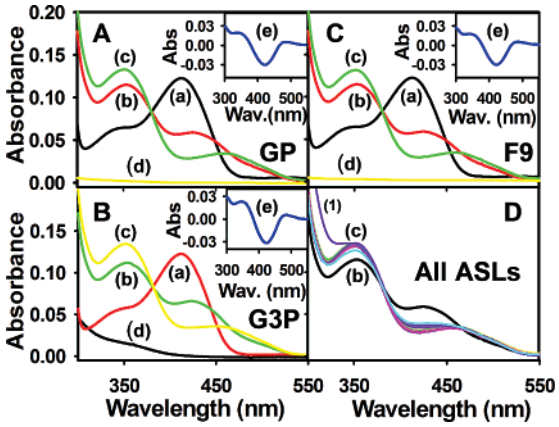

FIGURE 2: Influence of α-site ligands (ASLs) on the static UV−vis absorbance spectra of E(Aex$_1$) and E(A−A). Representative spectra are shown for three different ASLs: GP, G3P, and F9 in panels A−C, respectively. Each of these ASLs shifts the distribution of intermediates at the β-site in favor of E(A−A) (spectrum c). In each panel (A−C), the spectra correspond to (a) 20 μM $\alpha\beta$ in TEA, (b) 20 μM $\alpha\beta$, 100 mM NaCl, and 40 mM L-Ser, (c) the mixture for spectrum b with 50 mM GP, 4 mM G3P, or 200 μM F9, (d) 50 mM GP, 4 mM G3P, or 200 μM F9 in TEA, and (e) the difference spectrum (c minus b). Panel D summarizes the spectra obtained (i.e., spectrum c in panels A−C) with each ASL that was investigated (GP, G3P, F6, F9, F12, F19, and TPGH). Spectrum 1 is the spectrum obtained with F21. Spectrum 2 is the same as spectrum b in other panels.

F6, F9, F12, F19, and F21. F12 (trace 1) has a slightly different absorbance spectrum in the region between 300 and 350 nm because it includes contributions from the absorbance of the ligand. When corrected for these contributions, the shift in the distribution of PLP forms to favor E(A−A) at the expense of E(Aex$_1$) is essentially the same for each ligand, provided the ligand concentration is at or near saturation.

Effects of Ligands on the Apparent Affinity of L*-Ser for* $\alpha_2\beta_2$. Panels A−C of Figure 3 show absorbance spectra of $\alpha_2\beta_2$ measured after the addition of increasing concentrations of L-Ser in the absence (A) and in the presence of G3P (B) or F21 (C). These titrations show a progression in the conversion of E(Ain) to the equilibrium mixture of E(Aex$_1$) and E(A−A) that is dependent on the structure of the ASL. The other ligands (F9, F12, F19, and GP, data not shown) were found to have effects similar to those of G3P or F21. Panel D shows the difference spectra calculated by subtraction of spectrum a from spectrum n measured in the absence of an ASL (spectrum 1) and in the presence of F6, TPGH, G3P, GP, F12, F9, F19, or F21 (spectra 2−9, respectively). F6 and TPGH do not seem to increase the affinity of L-Ser for the β-site of the bienzyme complex (Table 2). Plots of absorbance at 412 nm versus L-Ser concentration measured in the absence and presence of 4 mM G3P or 200 μM F21 are shown in panels A−C of Figure 4, respectively. The other ligands behave like G3P and F21. The apparent dissociation constants for L-Ser obtained in the absence and presence of these ligands are listed in Table 2. Except for F6 and TPGH, the enzyme has a significantly higher apparent binding affinity for L-Ser in the presence of the ASLs than in the absence.

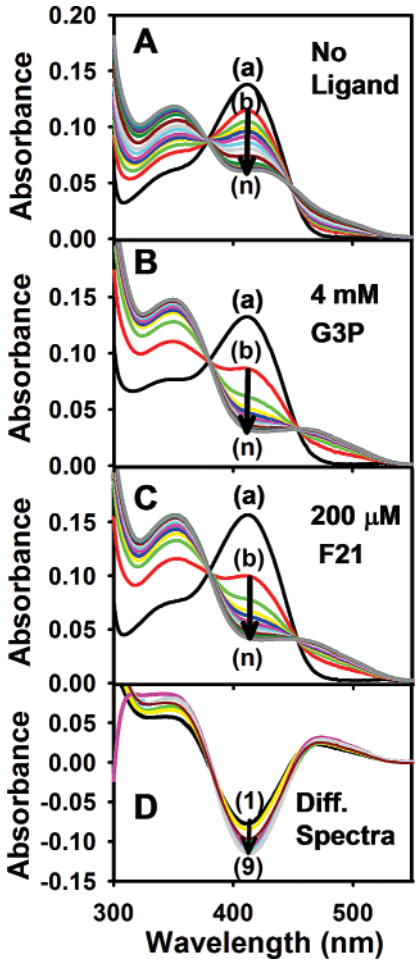

FIGURE 3: L-Ser titrations in the absence (A) and presence (B and C) of ASLs. Panels B and C show effects of 4 mM G3P and 200 μM F21, respectively, on E(Ain). Panel D presents the difference spectra between spectra a and n, labeled 1−9 with no ASL, 1 mM F6, 10 mM TPGH, 4 mM G3P, 50 mM GP, 200 μM F12, 200 μM F9, 200 μM F19, and 200 μM F21, respectively. The amount of E(Ain) decreases as the L-Ser concentration increases from 0 to 3230 μM. Reaction conditions: [$\alpha\beta$] = 20 μM, [NaCl] = 100 mM, [ligand] = 0, or 50 mM GP, or 200 μM F21, and [L-Ser] = 0, 25, 50, 74, 99, 146, 216, 307, 498, 1004, 1508, 2003, 2500, or 3002 μM. All experiments were carried out in 50 mM TEA buffer at pH 7.8.

Influence of Analogues on the Distribution of Species Formed in the Indoline Reaction. In Figure 5A, spectra a and b are the absorbance spectra of the indoline quinonoid intermediate, $E(Q)_{indoline}$, after the reaction of indoline with E(A−A) has reached equilibrium in the absence a and presence b of 4 mM G3P. In the absence of G3P (spectrum a), the spectrum is dominated by $E(Q)_{indoline}$ (λ_{max} = 466 nm), and in the presence of G3P (spectrum b and difference spectrum c), there is a small increase in the 466 nm band. These spectra show that the fraction of the enzyme in the form of $E(Q)_{indoline}$ increases in the presence of G3P.

Figure 5B shows that the binding of F9 also stabilizes $E(Q)_{indoline}$, and the extent of stabilization is similar to that caused by G3P. In other experiments, it was found that all the ASLs give a similar stabilization of $E(Q)_{indoline}$ except for TPGH. The binding of this ligand does not stabilize $E(Q)_{indoline}$.

Determination of Ligand Dissociation Constants by ANS Fluorescence. The fluorescence emission of ANS is strongly enhanced by binding to $\alpha_2\beta_2$ (*6*). The binding of ASLs decreases this fluorescence by displacement of ANS. Consequently, ANS can be used as a probe to quantify ligand binding (*6*, *18*, *20*, *23*). Figure 6 compares fluorescence spectra and titrations measured for the binding of GP (A and B) with the binding of F19 (C and D). Panels A and C of Figure 6 compare the effects of various concentrations of GP (Figure 6A, spectra b−h) or F19 (Figure 6C, spectra b−l) on the fluorescence emission spectrum of ANS. Panels B and D of Figure 6 show plots of the change in ANS fluorescence at 444 nm (values from panels A and C of Figure 6, respectively) as a function of the ligand concentration. To obtain the K_{Dapp} for GP and F19, these plots were fitted to the equation for a rectangular hyperbola (eq 2).

Similar measurements for the other ligands (G3P, TPGH, F6, F9, F12, and F21, data not shown) were performed in

Table 2: Summary of the Apparent Dissociation Constants, K_{Dapp}, and K_{Dapp}^{L-Ser}

	K_{Dapp} (μM) via ANS displacement		K_{Dapp}^{L-Ser}
	E(Ain)	E(A−A)	(L-Ser reaction) (μM)
no ASL			89.2 ± 11
GP	5700[a] ± 500	13.1[a] ± 4	11.5[a] ± 1
G3P	164[b] ± 40	3[b] ± 0.3	20.2[b] ± 3
F6	280 ± 50	38 ± 4	79.1 ± 5
F9	50 ± 5	1.84 ± 0.2	23.6 ± 3
F12	54.8 ± 11	4.55 ± 0.4	25.9 ± 2
F19	87.6 ± 9	3.26 ± 0.3	23.2 ± 2
F21	300 ± 83	18 ± 1	23.5 ± 1
TPGH	3000 ± 200	727 ± 250	70.2 ± 10

[a] Only one isomer of GP binds; therefore, the observed values have been corrected to reflect the D,L composition of the GP samples by multiplying by the factor 0.5. [b] Since it is the aldehyde form of G3P which binds, the observed values have been corrected for hydration to the gem diol form (96%) by multiplying by the factor 0.04/0.96 (45).

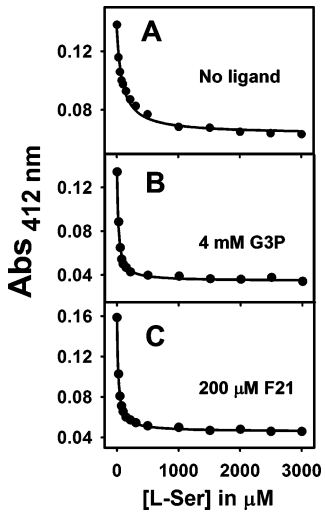

FIGURE 4: Representative isotherms showing the influence of ASLs on the reaction of L-Ser with E(Ain). Changes in absorbance at 412 nm are shown as a function of [L-Ser] both in the absence (A) of an ASL and in the presence of 4 mM G3P or 200 μM F21 (panel B or C, respectively). In each panel, the absorbance of E(Ain) at 412 nm decreases as [L-Ser] increases, with panels B and C showing sharper decreases in absorbance in comparison to panel A. K_{Dapp} values were obtained by fitting the data to the hyperbolic equation $A = [\text{L-Ser}](A_\infty - A_0)/(K_{Dapp} + [\text{L-Ser}])$, where A is the absorbance at 412 nm and A_∞ and A_0 are the absorbance values when [L-Ser] is ∞ and 0, respectively.

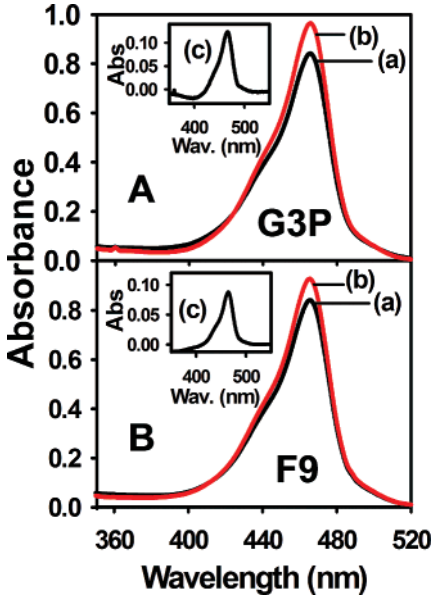

FIGURE 5: Static spectra showing the influence of G3P or F9 on $E(Q)_{indoline}$ at 466 nm. In each panel, spectrum a is the absorbance spectrum of $E(Q)_{indoline}$. Conditions: [$\alpha\beta$] = 17.4 μM, [NaCl] = 87 mM, [indoline] = 4 mM, and [L-Ser] = 35 mM. Spectrum b shows the absorbance spectrum of the solution of spectrum a with 4 mM G3P and with 174 μM F9 in panels A and B, respectively. In each panel, spectrum c shows the difference spectrum (b minus a).

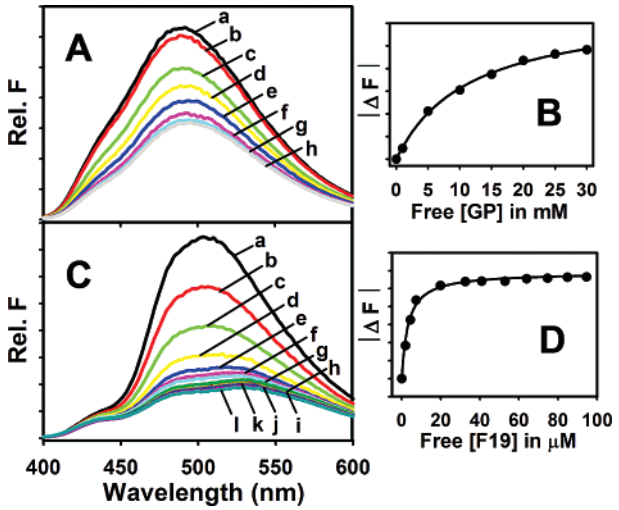

FIGURE 6: Influence of ASLs on the fluorescence of $\alpha_2\beta_2$-bound ANS. Representative spectra documenting the effects of an increasing ASL concentration on the displacement of ANS from the E(Ain)(ANS) complex are shown in panels A and B for GP, and panels C and D for F19. $|\Delta F|$ is the absolute value of the change in fluorescence. In panels A and B, the concentrations of GP were 0, 1, 5, 10, 15, 20, 25, and 30 mM, corresponding to spectra a−h, respectively. In panels C and D, the concentrations of F19 were 0, 5, 10, 15, 29, 42, 50, 62, 73, 84, 94, and 104 μM, corresponding to spectra a−l, respectively. Titrations were carried out as described in Materials and Methods. The K_{Dapp} values were calculated from the plots of free ASL concentration vs $|\Delta F|$ measured at 500 nm (panels B and D).

the presence of L-Ser, and apparent dissociation constants were similarly obtained (Table 2). All of the other ligands were found to behave like GP and F19. Table 2 summarizes the apparent dissociation constants measured for each ligand in the absence of L-Ser (left column) and in the presence of 40 mM L-Ser (middle column). In aqueous solution, G3P is

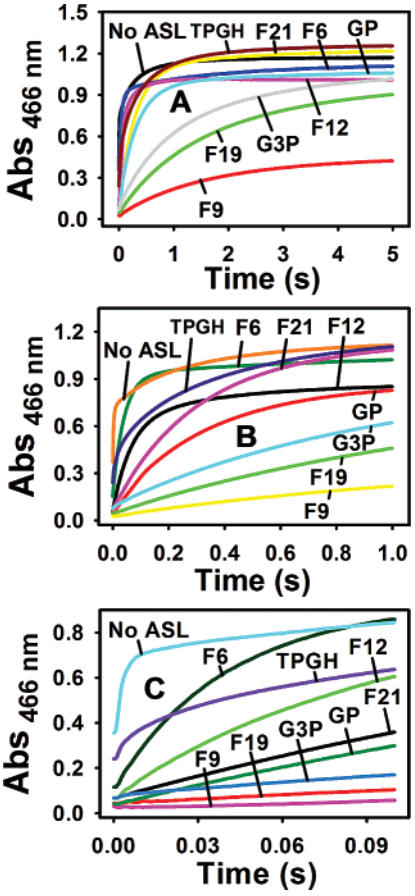

FIGURE 7: Representative stopped-flow rapid-mixing time courses are shown in panels A−C for three different time scales, 5 s, 1 s, and 100 ms, respectively. Each panel presents the kinetic time course for the appearance of the quinonoid intermediate measured in the absence of an ASL, for comparison with the time courses measured in the presence of the different ASLs. ASL concentrations were 50 mM GP, 5 mM G3P, and 10 mM TPGH, F6, F9, F12, F19, or F21. In a typical reaction, one syringe contains 20 μM $\alpha\beta$, 100 mM NaCl, and 40 mM L-Ser; the second syringe contains 10 mM indoline, 100 mM NaCl, and 40 mM L-Ser. When present, each syringe contained identical concentrations of the ASL.

extensively hydrated (96%, gem diol form) (*45*). Therefore, the K_{Dapp} values for G3P in Table 2 are corrected for hydration. This comparison shows that the K_{Dapp} values of the new ligands are comparable to that of the natural substrate, unhydrated G3P, and they bind much more tightly than GP does (Table 2).

Single-Wavelength Stopped-Flow (SWSF) Kinetic Studies

Influence of Analogues on the Indoline Reaction. Figure 7 presents kinetic time courses for the reaction of indoline with E(A−A) to give the indoline quinonoid intermediate, measured both in the absence and in the presence of F21, F6, GP, F12, TPGH, G3P, F19, or F9. These time courses show that in the absence of an ASL, the formation of the indoline quinonoid consists of a very fast phase with a large amplitude, followed by two slower phases with much smaller amplitudes. The fast phase arises from the nucleophilic attack of indoline on Cβ of the α-aminoacrylate double bond of E(A−A) (*8*, *12*, *46*); the slower phases have their origins in the conversion of $E(Aex_1)$ to E(A−A) and the interconversion of an inactive E(A−A) species to the active (*15*, *16*). In the presence of a saturating concentration of any one of

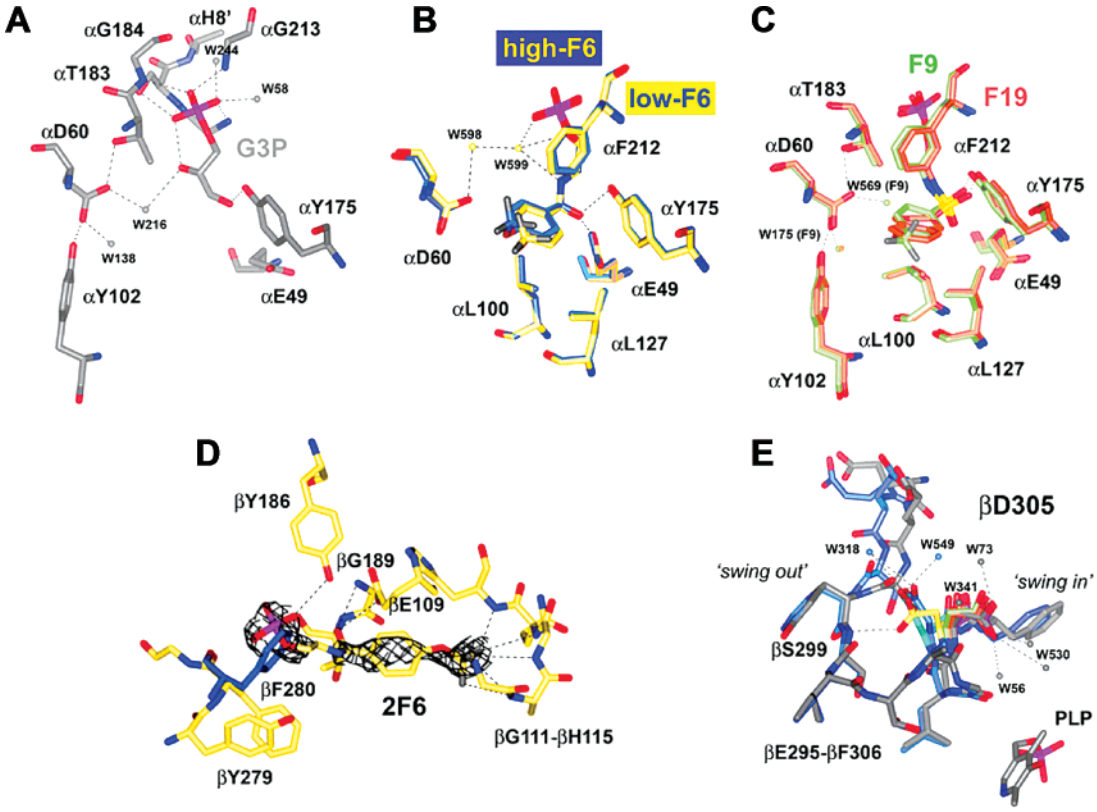

FIGURE 8: Structural comparisons. (A) Details of binding of G3P to the α-site (gray; the remaining coloration according to CPK atom type). (B) Overlay of low-F6 (light blue) and high-F6 (lemon) complexes. (C) Superposition of the F9 (light green) and F19 (coral) binding sites. (D) Structural details of the potential second F6 binding site in the high-F6 complex (lemon) with a superimposed σ_A-weighted $2F_o - F_c$ electron density map (cutoff of 1σ). The conformation of βPhe280 of the low-F6 complex is colored light blue. (E) Comparison of the conformations of βAsp305 in different E(Ain) structures. In addition to the investigated complexes (for color coding, see above) the conformation of βAsp305 in the IGP (cyan) and IPP (magenta) complexes (PDB entries 1QOQ and 1QOP, respectively) is displayed.

these ligands, the formation of $E(Q)_{indoline}$ is significantly slowed (Figure 7A). This phenomenon can clearly be seen in panels B and C of Figure 7, where the indoline reaction is monitored on relatively short time scales (1 s and 100 ms, respectively). F9 was found to have the strongest inhibitory effect on the rate of the indoline reaction (trace F9).

Crystal Structure of the G3P Complex with E(Ain). As expected, the structure of the G3P complex shows G3P bound to the α-site in a fashion that is similar to the binding of IGP (*23*, *47*, *48*) (Figure 8A) and also similar to the binding of GP to the βK87T and βS178P mutants (*24*, *49*). The phosphoryl of G3P (and of the other ASLs described below) binds at the same position that has been observed in the IGP or IPP complexes (PDB entries 1QOQ and 1QOP) and is engaged in a H-bonding network with residues αG234−αA236 of αH8′ (Figure 8A) and surrounding water molecules (*26*).

The 2′-hydroxyl group of G3P is the starting point for a network of H-bonds involving two water molecules and the catalytic residue, αAsp60. The OH group forms a hydrogen bond with Wat216 (3.2 Å), which interacts with Wat138 (2.8 Å) located next to the carboxylate OD2 atom of αAsp60 (2.7 Å). This atom (OD2) forms a H-bond with the hydroxyl group of αTyr102 (2.7 Å). The OD1 carboxylate atom of the catalytic αAsp60 forms H-bonds with Wat216 (2.7 Å) and the hydroxyl group of αThr183 (2.7 Å). The latter interaction results in complete closure of loop αL6. It is interesting to note that the carbonyl and hydroxyl groups of G3P are located at the same positions as the hydroxyls of 1-(2-hydroxyphenyl)amino-3-glycerol phosphate, a transition state analogue for the α-reaction (*18*). In this complex, the amino N (from 2AP) and the OH group at C3 form a H-bond with the OE1 and OE2 carboxylate atoms of αGlu49, thus holding the carboxylate in the active conformation. In the G3P complex (which is missing the amino group from 2AP), the carbonyl O atom of G3P cannot form a H-bond with the αGlu49 carboxylate, inducing the inactive conformation.

Crystal Structures of the F6 Complexes. Depending on the ligand concentration used for soaking the crystals before cryotrapping (see Materials and Methods), two different F6 complexes, designated as low-F6 and high-F6 complexes, were observed. In contrast to that for the G3P, F9, F19, and high-F6 complexes, the electron density for αL2, αL6, and the COMM domain were weak in the low-F6 complex, indicating high mobility. While the protein backbone of the low-F6 structure is traceable for most of the chain, the electron density of the side chain residues crucial for intersubunit communication (αL2 and βH6) or for closure of the α-site (αL6) is poorly defined. However, there is strong electron density for F6 itself in both the high- and low-F6 complexes. The positions of the trifluoromethoxyphenyl groups differ slightly in both F6 complexes (Figure 8B), corroborating the mobility of the F6 ligand.

Figure 8B shows details of the structures of F6 bound to the α-site. F6 binds at a position that is similar to several other ASLs (compare panels A and C of Figure 8). As mentioned above, the phosphoryl group is located at the same

position and forms the usual contacts; O6, one of the phosphoryl group oxygen atoms, O3, the bridging oxygen atom, and the F6 amide all form H-bonds with Wat599 (3.1 Å), which is 2.6 Å from Wat598 (high-F6 numbering). The latter forms a 3.0 Å H-bond with the OD1 carboxylate atom of αAsp60 that is barely visible in the low-F6 complex. Loop αL6 appears to be open and disordered in both F6 structures, possibly due to the location of two water molecules (Wat598 and Wat599) at the positions normally occupied by the OG1 (Δ 0.4 Å Wat598) and CG2 (Δ 1.2 Å Wat599) atoms of αThr183 in the closed conformation. Although the water molecules are well-defined in terms of electron density and do not completely overlap with the OG1 and CG2 atoms of αThr183, we cannot exclude the possibility of a closed conformation of the α-subunit where loop αL6 is too mobile to be visible in the electron density.

In both low- and high-F6 structures, the F6 amide carbonyl oxygen atom, O, forms a H-bond with the hydroxyl group of αTyr175 (2.7 and 3.0 Å for the low- and high-F6 complexes, respectively) in a manner analogous to that of the G3P complex. Additionally, there is a H-bond between the carbonyl O atom of F6 and the OE1 (2.3 Å) and OE2 (3.1 Å) carboxyl atoms of αGlu49 that is in the active conformation in all F6 complexes. This interaction implies that αGlu49 is protonated. The phenolic ring of F6 is sandwiched between αPhe212 and αLeu100, while αLeu127 is located in the plane of the ring. The terminal trifluoromethoxy group of F6 occupies a hydrophobic pocket made up by the side chains of αIle153, αLeu177, αPhe212, αLeu127, αAla129, and βPro18 at the subunit interface near the opening to the tunnel that connects the α- and β-sites.

Additional residual density was observed when the F6 complex was generated with high ligand concentrations. This new density indicates a second binding site for F6 within the αβ dimeric unit (Figure 8D). The second F6 molecule is located behind the so-called "gates" (βTyr278 and βPhe280) and pervades the tunnel. The F6 phosphoryl, the group with the highest electron density, occupies the position normally adopted by the phenyl ring of βPhe280 and pushes the ring into an alternative conformation rotated toward βTyr279 without impacting the main chain. The phosphoryl oxygen atoms, O5 and O6, form H-bonds with the hydroxyl of βTyr186 (3.2 Å) and the main chain oxygen of βPhe280 (2.7 Å), respectively. Parts of the trifluoromethoxy group are visible; this group makes contacts with a number of main chain atoms involving residues βGly111, βAla112, βGln114, and βHis115 in a pocket-like arrangement. The remainder of the ligand, including the phenyl ring, is poorly defined, indicating high mobility presumably because it lacks stabilizing interactions.

Crystal Structures of the F9 Complex. F9, G3P, and F6 all bind similarly to the enzyme (Figure 8A−C). However, there are significant differences in the F9 structure due to the interactions caused and provided by the different hybridizations of the sulfonamide sulfur and its substituent oxygens. This effect of hybridization results in different torsion angles of the chain between the phosphoryl group and the aromatic rings of F6 and F9. In particular, the F9 sulfonamide group is located above the phenyl ring of αPhe212 (CG 3.5 Å) and is oriented perpendicular to the plane of the carbamide group found in F6 (Figure 8B,C). This orientation results in an interaction with a water molecule, Wat569 (2.8 Å), which corresponds to Wat216 in the G3P structure, and which analogously forms a H-bond with the OD1 carboxylate atom of αAsp60 (2.6 Å). A second water, Wat175 (corresponding to Wat138 in the G3P complex), is H-bonded both to the OD2 carboxylate atom of αAsp60 (2.8 Å) and to the hydroxyl group of αTyr102 (2.7 Å). However, the two water molecules in the F9 complex are farther apart (4.2 Å) than in the (G3P)E(Ain) structure.

As observed in the G3P complex, the hydroxyl group of αThr183 forms a H-bond with αAsp60 (3.0 Å), resulting in a partially closed loop conformation of αL6 (visible up to αGly184). One of the F9 sulfonyl oxygens (O22) forms a hydrogen bond with the side chain hydroxyl of αTyr175 (2.5 Å), and the other one is close to the CG atom of αGlu49, which is in the inactive conformation.

Although the orientation of the trifluoromethoxy group is shifted by ∼1 Å toward αLeu127 compared to the F6 molecule in the low-F6 complex, the interactions of the phenyl and trifluoromethoxy groups of F9 resemble those in the F6 complex.

Crystal Structure of the F19 Complex. It is not surprising that the binding mode of F19 is similar to that of F9 as both ligands share similar functional groups, the sulfonylamido and phosphoryl groups, that mainly contribute to binding of F9. In the case of F19, the naphthalene ring system resides in nearly the same plane as the phenyl ring of F9 and is sandwiched among αPhe212, αLeu100, and αLeu127. The F19 complex exhibits all the structural features of the F9 complex, in particular the closed conformation of loop αL6 and the inactive conformation of αGlu49 (Figure 8C). All the aforementioned interactions for F9 (see above) are also observed in the F19 complex, although some distances differ slightly.

Impact of α-Site Ligand Binding on the β-Subunit. The overall β-subunit conformation is essentially the same in the addressed complexes and in the E(Ain) structures determined in the absence of ASLs (e.g., PDB entry 1KFK). However, it has been known for a long time that ASL binding leads to an ordering of some regions (β139−142, β158−β164, and βH6) within the COMM domain and to a repositioning of helix βH6 (β165−β181) (*26*, *49*). When the E(Ain) complexes with different ASLs are compared, small changes in the β-subunit within these regions are detected that appear to depend on ASL structure. While the G3P, F9, and F19 complexes superimpose well in all regards and are also in good agreement with the IPP-bound complex (*48*), both F6 complexes differ. While there is poor density in the case of the low-F6 complex for the side chains between β158 and β181, especially those involved in intersubunit communication with loop αL2, the main chain is clearly visible and its orientation resembles that observed in the IGP-bound structure (*48*). The main chain of the COMM domain of the low-F6 complex differs significantly compared to the G3P complex, leading to a maximum deviation of 1.7 Å (C_α βLys137) among residues β139−142 (located at the N-terminus of βH5) and of 2.7 Å (C_α βSer163) within the region of β158−164 (preceding helix βH6) (Figure 9). The high-F6 complex, however, exhibits a different behavior. In comparison with both the F9 and G3P complexes and the low-F6 complex, the high-F6 complex exhibits an intermediate conformation that deviates by 0.6 Å (C_α βLys137) and 0.8 Å (C_α βSer163) from the G3P complex.

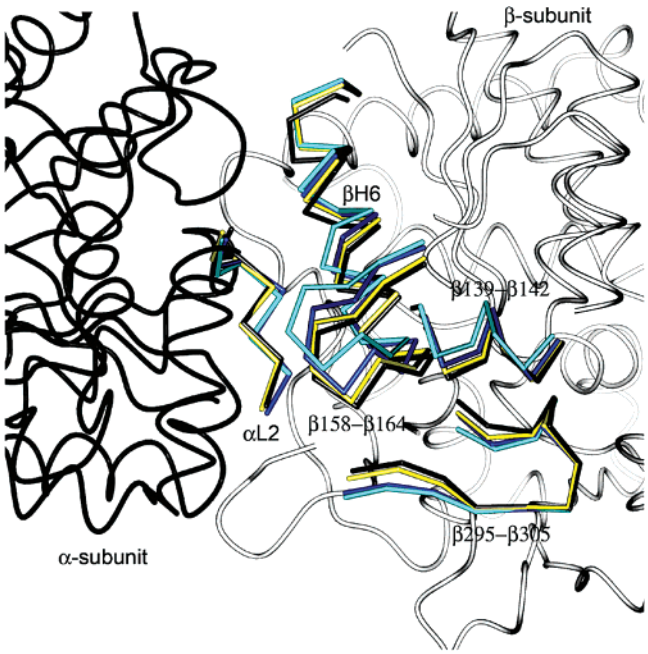

FIGURE 9: ASL-dependent shift of the β-site. The Cα traces of different tryptophan synthase structures are superimposed on the G3P-bound complex (in worm representation; α-domain colored black, β-domain colored light gray). Only those regions are displayed that were found to change upon ASL binding. The F9 and F19 complexes were omitted for clarity since they resemble the G3P-bound structure. Color coding: cyan for IGP (PDB entry 1QOQ), gray for G3P, light blue for the low-F6 complex, and lemon for the high-F6 complex.

A second difference involves the conformation of the carboxylate side chain of βAsp305 (Figure 8E). In the G3P, F9, and F19 complexes, the carboxylate group points toward the PLP ring system (as observed in the IPP complex) and interacts with a network of water molecules stabilized by the surrounding microenvironment, consisting mainly of main chain contacts.

In both F6 complexes, the βAsp305 carboxylate points away from the PLP ring system, the so-called "swing out" position (*49*, *50*), and interacts with either the amide of βSer299 (high-F6) or water molecules stabilized by main chain contacts originating from β295−306 (low-F6). A similar orientation was observed in the IPP-bound E(Ain) structure (*26*).

Except for the high-F6 complex, the positions of the gate residues (βTyr279 and βPhe280) are rather conserved in all structures. The Phe side chain within the high-F6 complex is flipped toward the Tyr ring, a conformation so far observed only in the ASL-free E(Ain) structure at room temperature (PDB entry 2WSY). Additionally, since there is residual density of what could be an alternate conformation of either residue, both residues appear to be somewhat mobile in the low-F6 complex.

DISCUSSION

Ligand-Mediated Allosteric Transitions in Tryptophan Synthase. The regulation of substrate channeling in the tryptophan synthase bienzyme complex depends upon the switching of $\alpha\beta$ dimeric units between open conformations of low catalytic activity and closed conformations of high activity (*6*). The switching between conformation and activity states is modulated by binding of substrate to the α-site and covalent transformations at the β-site (*8*, *9*, *12*, *13*, *21*, *32*). Investigations of allosteric interactions originating from binding of substrate to the α-site have been hampered by three happenstances. (a) Because the physiological α-site allosteric effector, IGP, is also the substrate for the α-site, studies of IGP binding are complicated by IGP cleavage. (b) IGP is expensive and inconvenient to prepare, and preparations are not chemically very stable. (c) Previously studied IGP analogues (i.e., IPP and IAG) do not have spectroscopic signatures of binding that are easily studied (*25*, *26*, *51*). The most frequently used G3P analogue, D,L-α-glycerol phosphate (GP), introduces some ambiguity because the commercially available material is a D,L mixture and is contaminated with the β-isomer, and GP binds relatively weakly to the α-site. The new sets of ASLs described in this report are designed to remedy these impediments.

Designing Ligands. The rapid cleavage of IGP to indole and G3P has made it difficult to disentangle the allosteric effects arising from the binding of IGP and G3P. Therefore, the analogues selected for synthesis in this work (Figure 1) were designed to be unreactive, while retaining a structural similarity to either IGP or G3P. The syntheses involve simple, single-step reactions, and purification is easy and fast, allowing efficient separation of product from starting materials and side products. This convenience of synthesis allows incorporation of spectroscopic probes (here exemplified by ASLs with ^{19}F groups for use as probes for ^{19}F NMR spectroscopy). Five of the analogues (F6, F9, F12, F19, and F21) have a terminal phosphoryl group connected to an aromatic ring by an aliphatic linker, giving structures with dimensions approximately the same as those of IGP. Because of the nature of the linker and the bonding to the aromatic ring, these five IGP analogues exhibit varying degrees of flexibility and different geometries. The sixth ASL (TPGH) is a structural analogue of G3P constructed from reaction of monochloroacetohydroxamic acid with sodium thiolphosphate. This analogue binds to the α-site with an affinity that is significantly weaker than the affinities of the analogues with aromatic groups (Table 2). The results presented in Figures 1−7 and Table 2 show that the new aromatic analogues exhibit relatively high affinities for the α-site and mimic the allosteric properties of other IGP analogues, including IPP (*25*), IAG (*51*), and GP (*8*, *44*). The behavior of G3P (*9*) and GP (*8*) is partially mimicked by the G3P analogue, TPGH. Consequently, these new compounds appear to be useful ASLs for probing allosteric mechanism in the tryptophan synthase system.

X-ray Crystallography. The crystal structures of the F9, F6, and F19 complexes (Figure 8) show that these ligands bind with high specificity to the α-site of the $\alpha\beta$ dimeric units of $\alpha_2\beta_2$. When F9 binds to the E(Ain) complex (Figure 8C), the α-site assumes a closed conformation. The trifluoromethoxy group of F9 extends into the opening of the 25 Å long tunnel at the α−β subunit interface. The structure of the F6 complex (Figure 8B) shows a binding mode similar to that of F9, but with interesting differences.

α-Subunit Conformation and Loop Dynamics Are Influenced by ASL Structure. The crystal structures of tryptophan synthase complexed with the ASLs, G3P, F6, F9, and F19 (Figure 8A−C) demonstrate how these ligands influence the conformation of the α-subunit. Previously, it has been shown

that complete closure of loop αL6 is required for creation of a well-ordered structural environment of the α-site (*18*, *23*, *24*, *26*, *48*, *49*) that promotes catalysis and enables the shuttling of indole through the tunnel after cleavage of IGP.

Comparison of the crystal structures of the ASL complexes indicates that when the α-site is occupied by GP, F9, or F19, loop αL6 is partially disordered, indicating it may not be completely closed, whereas G3P induces a completely closed conformation of this loop. In all these complexes, αGlu49 takes up an inactive conformation. The placement of the sulfonyl groups of F19 and F9 disfavors an active conformation of αGlu49 due to electrostatic repulsion. In the case of G3P, the product of the α-reaction (Scheme 1), the ligand is unable to hold αGlu49 in its active conformation. Conversion of the 3′-hydroxyl of IGP to the carbonyl of G3P eliminates the H-bonds to the αGlu49 carboxylate. Consequently, the αGlu49 carboxylate must switch to an alternative position to avoid an unfavorable electrostatic interaction with the G3P carbonyl oxygen. The switching of the αGlu49 carboxylate to the inactive conformation is reasonable from a mechanistic point of view, as αGlu49 is neither required in the further progress of the reaction nor involved in modulation of the α-site conformation.

In contrast, the F6 complexes display a more open, disordered αL6 but, uncharacteristically, an active conformation of αGlu49. Although αL6 closure has been correlated with both allosteric signaling and activation and positioning of the catalytic αAsp60 (*23*), it is only recently that the structural basis for loop closure has been addressed in detail and traced to the exact positioning of the side chain of αAsp60 (*18*). The structures described here support this finding and show that the interaction with the indolyl nitrogen, or a structural analogue, is not required for loop closure. Since αL6 should remain in the closed conformation in the G3P complex (after cleavage of IGP) to facilitate the subsequent transfer of indole to the *β*-active site, retention of the closed conformation makes sense in terms of the enzymatic mechanism. Compared to the IGP-bound and IGP-like-bound states observed in several structures (PDB entries 1QOQ, 1K8Z, and 1KF8, and in IGP complexes at different pHs, unpublished results), the conformation of αAsp60 differs slightly for all ASL complexes investigated in this study. The interaction between GP (*23*) and αAsp60, postulated to be one of the main contacts involved in loop closure, is mediated by a water molecule (Wat216 in the G3P structure) that is positioned by a H-bond with the 2-hydroxyl of G3P. There are homologous water molecules in the F9 and F19 complexes (Wat569 and Wat545, respectively), which similarly promote loop closure. This water molecule is located approximately ∼0.6 Å from the position of the CD1 ring atom in the analogous IGP complex. While the F6 complex has αAsp60 in the correct orientation for loop closure, αL6 appears to remain open. However, it is unclear from the structure of the F6 complex if the loop is disordered or just loosely closed and thus too mobile to be observable in the electron density.

We have shown previously, by kinetic and structural analysis of the isosteric αThr183Val mutant, that the H-bond between αThr183 and αAsp60 is crucial for loop closure (*23*). The structures of the ALS complexes described here highlight the importance of the water structure in the α-site for the allosteric signaling, providing a new twist to the intricate network of interactions in tryptophan synthase.

The structures presented in this work show that the conformation of the α-subunit is dependent on the ASL structure (compare the G3P, F6, F9, and F19 complexes shown in Figure 8A−C) and correlates with the differences in affinity for the different analogues (Table 2). The structures of the G3P, F9, and F19 complexes are similar, and the apparent affinity for G3P corrected for hydration is comparable to the affinities of F9 and F19.

While F6 has been shown to bind to the α-site, the binding of F6 does not induce the same structuring of the site that occurs in the F9 and F19 complexes. In contrast to the latter complexes, there is no well-defined electron density for αL6 in either F6 structure. Additionally, αL2 appears to be more mobile (side chains are less defined in terms of electron density) in the low-F6 complex. While this lack of structuring has further repercussions for the intersubunit communication (see below), the mobility of the α-site may be the structural basis for the 3- and 6-fold decreases in affinity compared to those of F9 and F19, respectively. Interestingly, the F6 complex shares more structural features with the IGP complex (αL6 open), which exhibits a similar αL2 mobility (as reflected in increased temperature factors).

Apparent Binding Affinities. The fluorescence of ANS strongly increases when ANS binds to hydrophobic protein surfaces (*52*). ANS binds to tryptophan synthase, and the shifting of the emission maximum suggests that ANS binds to a hydrophobic region (*21*). When ligands bind to either the α-site or the *β*-site, the ANS fluorescence decreases, indicating that ANS is displaced by a ligand-mediated conformational change of the enzyme (*21*). Figure 6 demonstrates that the binding of the new ASLs to the α-site also displaces ANS from the enzyme, causing a decrease in ANS fluorescence. Previous work (*9*) has shown that the reaction of L-Ser at the *β*-site increases ASL affinity. The effect of L-Ser on the apparent dissociation constant for each of the ASLs is shown in Table 2. These data establish that reaction of L-Ser at the *β*-site changes the affinity of the new ASLs for the α-site 25 Å away, and conversely, binding of the new ASLs to the α-site stabilizes E(A−A) at the *β*-site. The extent to which the affinity of the α-site for ASLs is enhanced by the reaction of L-Ser at the *β*-site exhibits a considerable dependence on the structure of the ASL. This effect appears to be much greater for GP, G3P, F9, F12, F19, or F21 than for TPGH or F6.

Allosteric Effects on the Distribution of Intermediates in Stage I of the β-Reaction. At pH 7.8, in stage I of the *β*-reaction for the Na^+ form of the enzyme, L-Ser reacts with the *β*-site to give comparable amounts of $E(Aex_1)$ and E(A−A) at equilibrium (*43*, *44*). The binding of the IGP analogues, IPP, IAG, and GP to the α-site alters the distribution of $E(Aex_1)$ and E(A−A), in favor of the E(A−A) intermediate (Figure 2D) (*8*, *14*, *44*, *51*, *53*). Figure 2D shows that TPGH, F6, F9, F12, F19, and F21 cause similar allosteric effects on the distribution of E(A−A) and $E(Aex_1)$. F9, F12, F19, and F21 cause similar decreases in the apparent dissociation constant for L-Ser binding, while the effects of F6 and TPGH are small (Table 2).

ASL Binding Modulates the Conformation of the β-Site. ASL binding gives complexes that influence the dynamics, conformation, and catalytic properties of the *β*-site (*6*−*8*,

17, *49*). This allosteric signaling is mediated through the conformations of α-subunit loops αL2 and αL6 and the COMM domain of the *β*-subunit (*9*, *11*, *18*, *23*, *24*, *26*, *49*, *54*). We conclude that in solution the differences in the apparent affinity of L-Ser for the *β*-site (Table 2) in the presence of ASLs arise from the different impact of the ligands on the structural sensors at the α-site that are involved in forwarding a structural signal to the *β*-site. In the crystalline state, the overall structure of the *β*-subunit is conserved in all of the ASL complexes that have been investigated. In these complexes, the *β*-subunit retains a relatively open conformation, but with small changes in some regions within the COMM domain in response to ASL binding.

When αL2 becomes ordered upon ASL binding, it forms an extensive H-bonding network with *β*H6 (residues *β*Pro165−*β*Ser178) (*26*) that leads to a reorientation of the helix. The positioning of *β*Ser178 was also shown to be responsible for loop closure of αL6 (*24*, *27*, *51*) through the H-bonding interaction between *β*Ser178 and αGly181. Careful comparisons of the E(Ain) complexes with G3P, IGP (PDB entry 1QOQ), IPP (PDB entry 1QOP), F6, F9, and F19 show that further ligand-dependent changes in the architecture of the *β*-subunit can be attributed to residues *β*139−142, *β*158−164, and, to a minor degree, *β*295−297. While the IPP, G3P, F9, and F19 complexes are very similar with well-defined conformations, they differ from both F6 and the IGP complexes which appear to be more flexible and less rigid (Figure 9), reflecting the structural dynamics of the IGP and F6 complexes. Although the IGP and low-F6 complexes are rather similar, the high-F6 structure exhibits an "intermediate" structure between the IPP-like and IGP-like structures. This intermediate structure is most likely induced by the binding of the second F6 in the tunnel (Figure 8D).

We conclude that the ability of an ASL to reorganize the *β*-active site correlates with the ability of the ASL to structure the α-site, and this structuring is conveyed to the *β*-subunit via the αL2−*β*H6 networking.

Only those ASLs that exhibit an IPP-like conformation on the structural level (e.g., G3P, F9, and F19) display an elevated affinity for L-Ser at the *β*-site (Table 2). While the reorganization of the *β*-domain in general can be attributed to the ASL-induced structuring of the α-site, the effect of ASL on the roles played by *β*Asp305 in *β*-site catalysis and substrate specificity (*26*, *49*, *50*, *55*) needs to be assessed. The *β*Asp305 carboxylate is oriented toward the PLP binding site and coordinated by a similar water network in the G3P, F9, and F19 complexes (Figure 8E). Interestingly, the *β*Asp305 carboxylate has a different orientation in both the F6 and IGP complexes. By comparison of the different E(Ain) structures that have been determined with IGP or IPP/GP (PDB entries 1QOP, 1KFC, and 1K8Y for IPP/GP and 1QOQ and 1KFB for IGP), we conclude that the orientation of the *β*Asp305 carboxylate directly depends on ligand structure (and its effects on the α-site) and does not depend on αL6 closure. When directed toward PLP, the *β*Asp305 carboxylate assumes the position in which it normally H-bonds to the hydroxyl group of the E(Aex_1) intermediate (e.g., see PDB entry 1KFJ). Mutational studies of *β*Asp305 have linked the side chain carboxylate to substrate recognition, substrate specificity, and nucleophile reaction specificity (*50*, *55*). It was shown that the *β*D305A mutant slows the formation of the E(Aex_1) species 3−15-fold compared to the wild-type enzyme. The absence of the carboxylate alters the interaction of L-Ser with the *β*-subunit and impairs formation of the E(Aex_1) species. Therefore, we propose that the correct orientation of the *β*Asp305 carboxylate contributes to the binding and reaction of L-Ser at the *β*-site, which would further explain the finding that F6 binding does not significantly increase the level of L-Ser binding (Table 2). It is interesting to note that the structure of the (F6)E(Aex_1) complex (*31*) shows that the *β*Asp305 carboxylate "swings in" and H-bonds to the hydroxyl of the L-Ser moiety and adopts a more IPP-like conformation without closing αL6.

*Modulation of the Switch to the Closed Conformation of the α*β*-Dimeric Unit*. The experiments of Dunn et al. (*8*) were the first to demonstrate that the route of entry of indole and indole analogues from solution into the *β*-site for reaction with E(A−A) is through the α-site and down the tunnel into the *β*-site. The key experiment involved demonstration that the binding of an ASL (GP) to the α-site strongly inhibits the rates, but not the yields, of $E(Q)_{Nu}$ formation when indole or indole analogues react with E(A−A). These experiments were the first to directly demonstrate the functional properties of the interconnecting tunnel and the switching of the α*β* dimeric unit between open and closed conformational states in response to the formation of E(A−A) at the *β*-site and to the binding of an ASL to the α-site (*8*). This work was extended and amplified in a series of subsequent studies (*9*−*11*, *13*−*17*, *20*, *56*, *57*). Consequently, the inhibitory effects of ASLs on the reaction of indole and indole analogues with E(A−A) have become a signature of the allosteric behavior of tryptophan synthase. The time courses presented in Figure 7 compare the effectiveness of the new ASLs with the behavior of GP and G3P on the inhibition of the rate of $E(Q)_{indoline}$ formation. These data establish that the new ASLs exhibit varying degrees of effectiveness in triggering the switch to the closed conformation of the α*β* dimeric unit, and this comparison also shows that the effectiveness is strongly dependent on ASL structure but does not correlate well with ASL binding affinities (Table 2). The mechanistic reasons for this lack of correlation will be the subject of future investigations.

L-Serine Binding in the Absence of ASLs Alters the α*-Site*. The finding that binding of L-Ser to the *β*-site increases the affinity of the α-site for ASLs (Table 2) supports our hypothesis that binding of either substrate to its binding site leads to a structuring of one site which subsequently increases the rigidity of the other subunit via intersubunit communication. Hence, adoption of a conformation that is already primed for binding instead of inducing the conformation by ligand binding itself leads to an increase in the affinity for the ligand. From comparison of the structures of different E(Aex_1) (ligand free) complexes, we predict that *β*Asp305 and the release of *β*Lys87 are involved in signaling the formation of the E(Aex_1) complex to *β*H6 which impacts the α-site by the ordering of αL2.

α*-Site*−*β-Site Allosteric Communication*. The α- and *β*-subunits of tryptophan synthase have a special way of communicating during the process of L-Trp synthesis. For efficient channeling, the reaction at the α-site must occur in phase with the reaction at the *β*-site (*6*, *13*, *17*). Synchronization is achieved by activating the α-site when E(Aex_1) is

converted to E(A−A) and then deactivating the α-site when $E(Q_3)$ is converted to $E(Aex_2)$ (*9*, *12*, *13*, *56*) (Scheme 1B). This conformational switching also insures that αβ subunit pairs remain in the closed conformation as E(A−A) is converted to $E(Aex_2)$. "Lids" in the α- and β-subunits control the conformation of both subunits, isolating the sites and the tunnel from solution and trapping indole within the confines of the α- and β-sites and the interconnecting tunnel. Consequently, indole is constrained to react with E(A−A) in the β-site. Following reaction of indole with E(A−A), the lids open again when $E(Q_3)$ is converted to $E(Aex_2)$ with subsequent release of G3P. The catalytic cycle for synthesizing L-Trp is then completed by conversion of $E(Aex_2)$ via $E(GD)_2$ to E(Ain), species with predominantly open conformations.

In this work, representative examples of four new classes of IGP analogues (aryl amides, aryl sulfonamides, aryl thioureas, and thiol phosphoglycolohydroxamate) have been successfully synthesized and characterized (Figure 1). Each of the representatives exerts strong effects on the allosteric communication between the α- and β-sites (Figures 2−5 and 7). The specific analogues chosen for this study bind more tightly to the bienzyme complex than GP does (Table 2) (*8*). Solution studies and the X-ray crystal structures show that these ligands bind with high specificity to the α-site and exert strong allosteric effects on the chemistry at the β-site (Figures 2 and 5). Binding of these ASLs drives the α-site to closed conformations. Conversion to the closed conformations at the α-site generates an allosteric signal that favors the closing of the β-site (*9*, *17*, *20*, *44*), thereby increasing the apparent affinity of the β-site for L-Ser (Table 2 and Figure 3) (*9*) and shifting the distribution of intermediates in favor of E(A−A) (Figure 2). These effects all result from ligand-mediated allosteric communication between the α- and β-sites in the complex (*9*−*13*, *16*−*21*, *32*, *44*).

CONCLUSIONS

This work reports the synthesis and characterization of six new ligands for tryptophan synthase representing four new classes of ASLs that mimic the allosteric properties of previously studied analogues for IGP and G3P (e.g., IPP, IAG, and GP). The syntheses of these ASLs are simple and allow the incorporation of spectroscopic probes for use in the investigation of the allosteric regulation of substrate channeling in the tryptophan synthase system.

REFERENCES

1. Yanofsky, C., and Crawford, I. P. (1972) Tryptophan Synthase, in *The Enzyme* (Boyer, P. D., Ed.) 3rd ed., pp 1−31, Academic Press, New York.
2. Miles, E. W. (1979) Tryptophan synthase: Structure, function, and subunit interaction, *Adv. Enzymol. Relat. Areas Mol. Biol. 49*, 127−186.
3. Miles, E. W. (1991) Structural basis for catalysis by tryptophan synthase, *Adv. Enzymol. Relat. Areas Mol. Biol. 64*, 93.
4. Miles, E. W. (1995) Tryptophan synthase. Structure, function, and protein engineering, *Subcell. Biochem. 24*, 207−254.
5. Miles, E. W., Rhee, S., and Davies, D. R. (1999) The molecular basis of substrate channeling, *J. Biol. Chem. 274*, 12193−12196.
6. Pan, P., Woehl, E., and Dunn, M. F. (1997) Protein architecture, dynamics and allostery in tryptophan synthase channeling, *Trends Biochem. Sci. 22*, 22−27.
7. Hyde, C. C., Ahmed, S. A., Padlan, E. A., Miles, E. W., and Davies, D. R. (1988) Three-dimensional structure of the tryptophan synthase $\alpha_2\beta_2$ multienzyme complex from *Salmonella typhimurium*, *J. Biol. Chem. 263*, 17857−17871.
8. Dunn, M. F., Aguilar, V., Brzovic, P., Drewe, W. F., Jr., Houben, K. F., Leja, C. A., and Roy, M. (1990) The tryptophan synthase bienzyme complex transfers indole between the α- and β-sites via a 25−30 Å long tunnel, *Biochemistry 29*, 8598−8607.
9. Brzovic, P. S., Ngo, K., and Dunn, M. F. (1992) Allosteric interactions coordinate catalytic activity between successive metabolic enzymes in the tryptophan synthase bienzyme complex, *Biochemistry 31*, 3831−3839.
10. Brzovic, P. S., Sawa, Y., Hyde, C. C., Miles, E. W., and Dunn, M. F. (1992) Evidence that mutations in a loop region of the α-subunit inhibit the transition from an open to a closed conformation in the tryptophan synthase bienzyme complex, *J. Biol. Chem. 267*, 13028−13038.
11. Brzovic, P. S., Hyde, C. C., Miles, E. W., and Dunn, M. F. (1993) Characterization of the functional role of a flexible loop in the α-subunit of tryptophan synthase from *Salmonella typhimurium* by rapid-scanning, stopped-flow spectroscopy and site-directed mutagenesis, *Biochemistry 32*, 10404−10413.
12. Leja, C. A., Woehl, E. U., and Dunn, M. F. (1995) Allosteric linkages between β-site covalent transformations and α-site activation and deactivation in the tryptophan synthase bienzyme complex, *Biochemistry 34*, 6552−6561.
13. Anderson, K. S., Miles, E. W., and Johnson, K. A. (1991) Serine modulates substrate channeling in tryptophan synthase-A novel intersubunit triggering mechanism, *J. Biol. Chem. 266*, 8020−8033.
14. Woehl, E., and Dunn, M. F. (1999) Mechanisms of monovalent cation action in enzyme catalysis: The first stage of the tryptophan synthase β-reaction, *Biochemistry 38*, 7118−7130.
15. Woehl, E., and Dunn, M. F. (1999) Mechanisms of monovalent cation action in enzyme catalysis: The tryptophan synthase α-, β-, and αβ-reactions, *Biochemistry 38*, 7131−7141.
16. Weber-Ban, E., Hur, O., Bagwell, C., Banik, U., Yang, L. H., Miles, E. W., and Dunn, M. F. (2001) Investigation of allosteric linkages in the regulation of tryptophan synthase: The roles of salt bridges and monovalent cations probed by site-directed mutation, optical spectroscopy, and kinetics, *Biochemistry 40*, 3497−3511.
17. Harris, R. M., and Dunn, M. F. (2002) Intermediate trapping via a conformational switch in the Na^+-activated tryptophan synthase bienzyme complex, *Biochemistry 41*, 9982−9990.
18. Kulik, V., Hartmann, E., Weyand, M., Frey, M., Gierl, A., Niks, D., Dunn, M. F., and Schlichting, I. (2005) On the structural basis of the catalytic mechanism and the regulation of the α subunit of tryptophan synthase from *Salmonella typhimurium* and BX1 from maize, two evolutionarily related enzymes, *J. Mol. Biol. 352*, 608−620.
19. Osborne, A., Teng, Q., Miles, E. W., and Phillips, R. S. (2003) Detection of open and closed conformations of tryptophan synthase by ^{15}N-heteronuclear single-quantum coherence nuclear magnetic resonance of bound ^{15}N-L-tryptophan, *J. Biol. Chem. 278*, 44083−44090.
20. Harris, R. M., Ngo, H., and Dunn, M. F. (2005) Synergistic effects on escape of a ligand from the closed tryptophan synthase bienzyme complex, *Biochemistry 44*, 16886−16895.
21. Pan, P., and Dunn, M. F. (1996) β-Site covalent reactions trigger transitions between open and closed conformations of the tryptophan synthase bienzyme complex, *Biochemistry 35*, 5002−5013.
22. Sachpatzidis, A., Dealwis, C., Lubetsky, J. B., Liang, P. H., Anderson, K. S., and Lolis, E. (1999) Crystallographic studies of phosphonate-based α-reaction transition-state analogues complexed to tryptophan synthase, *Biochemistry 38*, 12665−12674.
23. Kulik, V., Weyand, M., Seidel, R., Niks, D., Arac, D., Dunn, M. F., and Schlichting, I. (2002) On the role of αThr183 in the allosteric regulation and catalytic mechanism of tryptophan synthase, *J. Mol. Biol. 324*, 677−690.
24. Weyand, M., Schlichting, I., Marabotti, A., and Mozzarelli, A. (2002) Crystal structures of a new class of allosteric effectors complexed to tryptophan synthase, *J. Biol. Chem. 277*, 10647−10652.
25. Heyn, M. P., and Weischet, W. O. (1975) Circular dichroism and fluorescence studies on the binding of ligands to the α subunit of tryptophan synthase, *Biochemistry 14*, 2962−2968.
26. Schneider, T. R., Gerhardt, E., Lee, M., Liang, P. H., Anderson, K. S., and Schlichting, I. (1998) Loop closure and intersubunit communication in tryptophan synthase, *Biochemistry 37*, 5394−5406.

27. Marabotti, A., De, B. D., Tramonti, A., Bettati, S., and Mozzarelli, A. (2001) Allosteric communication of tryptophan synthase. Functional and regulatory properties of the βS178P mutant, *J. Biol. Chem. 276*, 17747−17753.
28. Collins, K. D. (1974) Activated intermediate analog: Use of phosphoglycolohydroxamate as a stable analog of a transiently occurring dihydroxyacetone phosphate-derived enolate in enzymatic catalysis, *J. Biol. Chem. 249*, 136−142.
29. Lolis, E., and Petsko, G. A. (1990) Crystallographic analysis of the complex between triosephosphate isomerase and 2-phosphoglycolate at 2.5-Å resolution: Implications for catalysis, *Biochemistry 29*, 6619−6625.
30. Casino, P., Niks, D., Ngo, H., Pan, P., Brzovic, P., Blumenstein, L., Barends, T. R., Schlichting, I., and Dunn, M. F. (2007) Allosteric regulation of tryptophan synthase channeling: The internal aldimine probed by *trans*-3-indole-3′-acrylate binding, *Biochemistry 46*, 7728−7739.
31. Ngo, H., Kimmich, N., Harris, R., Niks, D., Blumenstein, L., Kulik, V., Barends, T. R., Schlichting, I., and Dunn, M. F. (2007) Allosteric regulation of substrate channeling in tryptophan synthase: Modulation of the L-serine reaction in stage I of the β-reaction by α-site ligands, *Biochemistry 46*, 7740−7753.
32. Kawasaki, H., Bauerle, R., Zon, G., Ahmed, S. A., and Miles, E. W. (1987) Site-specific mutagenesis of the α subunit of tryptophan synthase from *Salmonella typhimurium*. Changing arginine 179 to leucine alters the reciprocal transmission of substrate-induced conformational changes between the α and β_2 subunits, *J. Biol. Chem. 262*, 10678−10683.
33. Miles, E. W., Bauerle, R., and Ahmed, S. A. (1987) Tryptophan synthase from *Escherichia coli* and *Salmonella typhimurium*, *Methods Enzymol. 142*, 398−414.
34. Miles, E. W., Kawasaki, H., Ahmed, S. A., Morita, H., Morita, H., and Nagata, S. (1989) The β-subunit of tryptophan synthase: Clarification of the roles of histidine-86, lysine-87, arginine-148, cysteine-170, and cysteine-230, *J. Biol. Chem. 264*, 6280−6287.
35. Yang, L., Ahmed, S. A., and Miles, E. W. (1996) PCR mutagenesis and overexpression of tryptophan synthase from *Salmonella typhimurium*: On the roles of β_2 subunit Lys-382, *Protein Expression Purif. 8*, 126−136.
36. Rowlett, R., Yang, L. H., Ahmed, S. A., McPhie, P., Jhee, K. H., and Miles, E. W. (1998) Mutations in the contact region between the α and β subunits of tryptophan synthase alter subunit interaction and intersubunit communication, *Biochemistry 37*, 2961−2968.
37. Jones, W. L., and Werner, F. L. (1916) Aliphatic hydroxylammonium salts and hydroxamic acids with halogen substituents, *J. Am. Chem. Soc. 38*, 413−422.
38. Duncan, R., and Drueckhammer, D. G. (1993) Phosphorothioate and phosphoramide analogs of dihydroxyacetone phosphate, *Tetrahedron Lett. 34*, 1733−1736.
39. Kabsch, W. (1993) Automatic processing of rotation diffraction data from crystals of initially unknown symmetry and cell constants, *J. Appl. Crystallogr. 26*, 795−800.
40. Brunger, A. T., Adams, P. D., Clore, G. M., Delano, W. L., Gros, P., Grosse-Kunstleve, R. W., Jiang, J. S., Kuszewski, J., Nilges, M., Pannu, N. S., Read, R. J., Rice, L. M., Simonson, T., and Warren, G. L. (1998) Crystallography & NMR system: A new software suite for macromolecular structure determination, *Acta Crystallogr. D54*, 905−921.
41. Jones, T. A., Zou, J. Y., Cowan, S. W., and Kjeldgaard, M. (1991) Improved methods for building protein models in electron-density maps and the location of errors in these models, *Acta Crystallogr. A47*, 110−119.
42. McRee, D. E. (1999) XtalView Xfit: A versatile program for manipulating atomic coordinates and electron density, *J. Struct. Biol. 125*, 156−165.
43. Drewe, W. F., Jr., and Dunn, M. F. (1985) Detection and identification of intermediates in the reaction of L-serine with *Escherichia coli* tryptophan synthase via rapid-scanning ultraviolet-visible spectroscopy, *Biochemistry 24*, 3977−3987.
44. Houben, K. F., and Dunn, M. F. (1990) Allosteric effects acting over a distance of 20−25 Å in the *Escherichia coli* tryptophan synthase bienzyme complex increase ligand affinity and cause redistribution of covalent intermediates, *Biochemistry 29*, 2421−2429.
45. Trentham, D. R., McMurray, C. H., and Pogson, C. I. (1969) Active chemical state of D-glyceraldehyde 3-phosphate in its reactions with D-glyceraldehyde 3-phosphate dehydrogenase, aldolase and triose phosphate isomerase, *Biochem. J. 114*, 19.
46. Roy, M., Keblawi, S., and Dunn, M. F. (1988) Stereoelectronic control of bond formation in *Escherichia coli* tryptophan synthase: Substrate specificity and enzymatic synthesis of the novel amino acid dihydroisotryptophan, *Biochemistry 27*, 6698−6704.
47. Rhee, S., Miles, E. W., and Davies, D. R. (1998) Cryocrystallography of a true substrate, indole-3-glycerol phosphate, bound to a mutant (αD60N) tryptophan synthase $\alpha_2\beta_2$ complex reveals the correct orientation of active site αGlu49, *J. Biol. Chem. 273*, 8553−8555.
48. Weyand, M., and Schlichting, I. (1999) Crystal structure of wild-type tryptophan synthase complexed with the natural substrate indole-3-glycerol phosphate, *Biochemistry 38*, 16469−16480.
49. Rhee, S., Parris, K. D., Hyde, C. C., Ahmed, S. A., Miles, E. W., and Davies, D. R. (1997) Crystal structures of a mutant (βK87T) tryptophan synthase $\alpha_2\beta_2$ complex with ligands bound to the active sites of the α- and β-subunits reveal ligand-induced conformational changes, *Biochemistry 36*, 7664−7680.
50. Ferrari, D., Yang, L. H., Miles, E. W., and Dunn, M. F. (2001) βD305A mutant of tryptophan synthase shows strongly perturbed allosteric regulation and substrate specificity, *Biochemistry 40*, 7421−7432.
51. Marabotti, A., Cozzini, P., and Mozzarelli, A. (2000) Novel allosteric effectors of the tryptophan synthase $\alpha_2\beta_2$ complex identified by computer-assisted molecular modeling, *Biochim. Biophys. Acta 1476*, 287−299.
52. Stryer, L. (1965) The interaction of a naphthalene dye with apomyoglobin and apohemoglobin. A fluorescent probe of non-polar binding sites, *J. Mol. Biol. 13*, 482−495.
53. Lane, A. N., and Kirschner, K. (1983) The mechanism of binding of L-serine to tryptophan synthase from *Escherichia coli*, *Eur. J. Biochem. 129*, 561−570.
54. Weyand, M., Schlichting, I., Herde, P., Marabotti, A., and Mozzarelli, A. (2002) Crystal structure of the β Ser178→ Pro mutant of tryptophan synthase. A "knock-out" allosteric enzyme, *J. Biol. Chem. 277*, 10653−10660.
55. Ferrari, D., Niks, D., Yang, L. H., Miles, E. W., and Dunn, M. F. (2003) Allosteric communication in the tryptophan synthase bienzyme complex: Roles of the β-subunit aspartate 305-arginine 141 salt bridge, *Biochemistry 42*, 7807−7818.
56. Kirschner, K., Lane, A. N., and Strasser, A. W. M. (1991) Reciprocal communication between the lyase and synthase active-sites of the tryptophan synthase bienzyme complex, *Biochemistry 30*, 472−478.
57. Lane, A. N., and Kirschner, K. (1991) Mechanism of the physiological reaction catalyzed by tryptophan synthase from *Escherichia coli*, *Biochemistry 30*, 479−484.

BI700385F